Syncytial basis for diversity in spike shapes and their propagation in detrusor smooth muscle

Appukuttan, Shailesh; Brain, Keith; Manchanda, Rohit

DOI:
10.1016/j.procs.2015.05.199

Document Version
Publisher's PDF, also known as Version of record

Citation for published version (Harvard):
Appukuttan, S, Brain, K & Manchanda, R 2015, 'Syncytial basis for diversity in spike shapes and their propagation in detrusor smooth muscle', *Procedia Computer Science*, vol. 51, pp. 785-794. https://doi.org/10.1016/j.procs.2015.05.199

Procedia Computer Science

Volume 51, 2015, Pages 785–794

ICCS 2015 International Conference On Computational Science

Syncytial Basis for Diversity in Spike Shapes and their Propagation in Detrusor Smooth Muscle

Shailesh Appukuttan[1], Keith Brain[2] and Rohit Manchanda[1]
[1]*Indian Institute of Technology Bombay, Mumbai, India*
[2]*University of Birmingham, Birmingham, U.K.*
shailesh.a@iitb.ac.in, k.l.brain@bham.ac.uk, rmanch@iitb.ac.in

Abstract
Syncytial tissues, such as the smooth muscle of the urinary bladder wall, are known to produce action potentials (spikes) with marked differences in their shapes and sizes. The need for this diversity is currently unknown, and neither is their origin understood. The small size of the cells, their syncytial arrangement, and the complex nature of innervation poses significant challenges for the experimental investigation of such tissues. To obtain better insight, we present here a three-dimensional electrical model of smooth muscle syncytium, developed using the compartmental modeling technique, with each cell possessing active channel mechanisms capable of producing an action potential. This enables investigation of the syncytial effect on action potential shapes and their propagation. We show how a single spike shape could undergo modulation, resulting in diverse shapes, owing to the syncytial nature of the tissue. Differences in the action potential features could impact their capacity to propagate through a syncytium. This is illustrated through comparison of two distinct action potential mechanisms. A better understanding of the origin of the various spike shapes would have significant implications in pathology, assisting in evaluating the underlying cause and directing their treatment.

Keywords: Syncytium, Gap Junction, Action Potentials, Spikes, Propagation

1 Introduction

Action potentials (APs) are electrical signals generated in excitable cells for inter-cellular communication and activation of intra-cellular processes. They are known to exist in a variety of shapes. For example, the action potential produced in the skeletal muscle is quite different from the cardiac action potential. But, generally, cells belonging to the same tissue tend to more or less follow a regular AP template. The smooth muscle of the urinary bladder, called the detrusor, is quite unique in these regards. It is found to exhibit action potentials of varying shapes and sizes (Hayase, Hashitani, Kohri, & Suzuki, 2009). These include: (a) marked differences in peak amplitudes and (b) width of the spikes, (c) differences in the shape of the spike 'foot', (d) extent of hyperpolarization, and (e) presence

Selection and peer-review under responsibility of the Scientific Programme Committee of ICCS 2015

doi:10.1016/j.procs.2015.05.199

or absence of after-depolarization. Most importantly, these variations in shapes are observed even in recordings obtained from a single cell. However, the origin of this diversity in spike shapes implores for a better understanding. Intuitively, two possibilities arise for their origin: (i) multiple spike generation mechanisms, or (ii) few spike generation mechanisms and their variable modulation.

This lack of clarity on bladder physiology is largely attributed to the complex nature of the detrusor environment. The detrusor smooth muscle (DSM) cells are known to form three-dimensional electrical syncytia by means of low-resistance electrical pathways between adjacent cells, through formation of gap junctions (Manchanda, 1995). This entails that electrical activity recorded from a particular cell need not necessarily have its origin in that cell, but could possibly have been initiated at any other cell within the electrical syncytium. Moreover, the response of a cell is influenced by the biophysical properties of other cells in the syncytium and the cell's location within it. The pattern of innervation further convolutes the setting. A single nerve terminal may innervate multiple DSM cells and likewise a single DSM cell may receive inputs from multiple nerve terminals (Manchanda, 1995).

In terms of function, the urinary bladder regulates both storage as well as voiding of urine. During the storage phase, localized contractions help the bladder in maintaining tone. In the voiding phase coordinated contractions of the bladder, along with relaxation of the urethra, results in emptying of the bladder. The localized contractions are believed to originate from spontaneous spiking of the cells, whereas coordinated contractions are a collective result of nerve-evoked spikes (Andersson, 2011). It is interesting to note the active role of spikes in both the phases. Traditionally, when spikes are analyzed, the focus predominantly lies in the frequency of spiking and most often the variations in the shape of the individual spikes are overlooked. The individual spike shapes potentially offer more insight into the actual underlying changes arising in pathology. For example, overactive bladder (OAB) is often associated with detrusor overactivity, wherein the detrusor undergoes unsolicited contractions arising from aberrant spiking. It is conceivable that pathological conditions affecting the mechanisms that restrict the spread of localized contractions into full-scale bladder contractions could lead to detrusor overactivity (Fry, Skennerton, Wood, & Wu, 2002). Here, we hypothesize that spike features play an important role in determining its ability to propagate throughout the bladder.

In view of the difficulties involved in the experimental investigation, a computational approach might assist in unraveling the origin of the signals. Prior modeling work on smooth muscle primarily consisted of analytical approaches, wherein governing equations for a particular network layout were developed and their solutions derived (Purves, 1976) (Bennett, Gibson, & Poznanski, 1993) (Sourav & Manchanda, 2000). Any change in the network required reworking of the equations and their solutions. An approach that offers much greater flexibility is the compartmental modeling approach (Rall, 1964). Here the cellular structures are divided into a number of small, interconnected compartments. The size of each compartment is restricted to a small fraction of the length constant, thereby allowing each compartment to be treated as being spatially isopotential. This eliminates spatial derivatives and reduces the governing PDEs into coupled time-dependent ODEs. While this approach has been widely employed in order to model neurons, it had not been applied to syncytial smooth muscle. Hence, our model of a passive smooth muscle syncytium (Appukuttan, Brain, & Manchanda, 2014) was the first of its kind. The model was rigorously validated against both theoretical predictions and experimental observations. Here, we have incorporated active mechanisms in this model to enable the study of the propagation and modulation of spike shapes. As the detrusor action potential follows no single template and the cells possess an array of 9 or more channels contributing to these spikes (Brading & Brain, 2011), models for the same have not yet been satisfactorily developed. The objective of the current work is to obtain insights into the syncytial nature as a basis for diversity in spike shapes and their capacity to propagate. We have utilized the classical Hodgkin-Huxley (HH) model along with an atrial spike model to demonstrate the same. Our aim is to shed light on two primary questions: (i) Does the syncytial organization of the cells contribute to the diversity in the exhibited spike shapes? (ii) Does the shape of the spike determine its extent of propagation within the syncytium?

2 Methods

A three-dimensional model of smooth muscle syncytium was developed on the NEURON simulation environment, a compartmental modeling platform (Carnevale & Hines, 2006). This primarily involved modeling the individual cells, their coupling via gap junctions and developing the topology of the syncytium, followed by equipping the desired cells in the syncytium with synaptic input.

2.1 Modeling the Syncytium

Individual smooth muscle cells are known to be fusiform in shape, and here, following past conventions, they have been approximated as long narrow cylinders 200 µm in length and 6 µm in diameter with axial resistivity of 183 Ω.cm based on experimental data (Fry, Cooklin, Birns, & Mundy, 1999) (Appukuttan, Brain, & Manchanda, 2014). All the cells were equipped with HH set of channels.

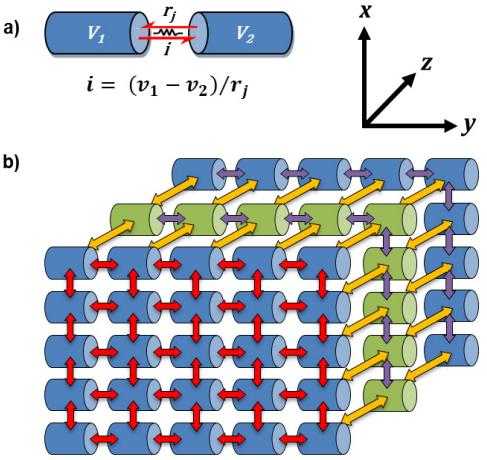

Figure 1: Simplified representations of (a) gap junction implementation in NEURON, (b) 3-D syncytium

Gap junctions were customarily modeled as resistive links connecting adjacent cells. In NEURON, this was achieved by means of point-processes, which allow insertion of localized conductances. A single bi-directional gap junction connecting two cells consists of two unidirectional constructs, with each cell hosting one apiece as shown in fig. 1(a). Each of the constructs keeps track of membrane potential changes in the connected cell. The potential difference between the cells, thus tracked, along with the value of gap junctional resistance allows evaluation of the gap junctional current to be inserted or removed from the host cell. These currents, naturally, are equal in magnitude but opposite in direction for the two cells and thus reflect the flow of current from one cell to another. The value of gap junctional resistance was derived from experimental data (Fry, Cooklin, Birns, & Mundy, 1999).

$$R_j = R'_j \text{ x} \frac{l}{\pi a^2} = 427 \text{ x } \frac{200 \text{ x } 10^{-4}}{\pi \text{ x } (3 \text{ x } 10^{-4})^2} = 30.2\ M\Omega \qquad \text{(Eq. 1)}$$

where R'_j is the specific gap junctional resistance, l is the cell length and a is the radius of the cell. This was later tuned to 30.6 MΩ to obtain a fit to other parameters (Appukuttan, Brain, & Manchanda, 2014).

Using the above means of electrically coupling cells, a three-dimensional model was developed with a simple cubic lattice arrangement of cells, as represented in fig. 1(b). The syncytium was aligned

such that the y-axis was along the length of the cells, and the x-z plane represented the cross-section of the cells. Each cell in the syncytium was coupled to six other adjacent cells, two along each axis. The size of the syncytium, unless otherwise specified, was set to 5-cube - roughly corresponding to experimental studies that have revealed functional syncytia containing up to 100 cells (Neuhaus, Wolburg, Hermsdorf, Stolzenburg, & Dorschner, 2002).

2.2 Modeling Synaptic Activity

Synaptic activity involves a localized conductance change in the membrane. It has been shown that the kinetics of this conductance change can be described mathematically using an 'alpha function', such as:

$$g(t) = \begin{cases} 0 & for\ t < t_{act} \\ g_{max} * \frac{(t - t_{act})}{\tau} * e^{\left(\frac{-(t - t_{act} - \tau)}{\tau}\right)} & for\ t \geq t_{act} \end{cases} \quad \text{(Eq. 2)}$$

where t_{act} is the time of synaptic activation and $g(t)$ attains its peak of g_{max} at $t = t_{act} + \tau$. The synaptic current is then evaluated by the expression:

$$i(t) = g(t) * \{V_m(t) - e\} \quad \text{(Eq. 3)}$$

where V_m is the membrane potential and e is the reversal potential of the synaptic current. Such representations have been widely employed in modeling (Jack, Noble, & Tsien, 1975) (Purves, 1976) (Bennett, Gibson, & Poznanski, 1993) and in NEURON these mechanisms are identified as AlphaSynapses. In our current study, AlphaSynapses have been employed as stimuli to initiate APs.

2.3 AP Parameters and their Measurements

As our study involves action potentials of diverse shapes and sizes, it is necessary to be able to distinguish and quantify these differences. This has been achieved here by evaluating the following 5 parameters for each spike shape, as illustrated in Fig. 2:

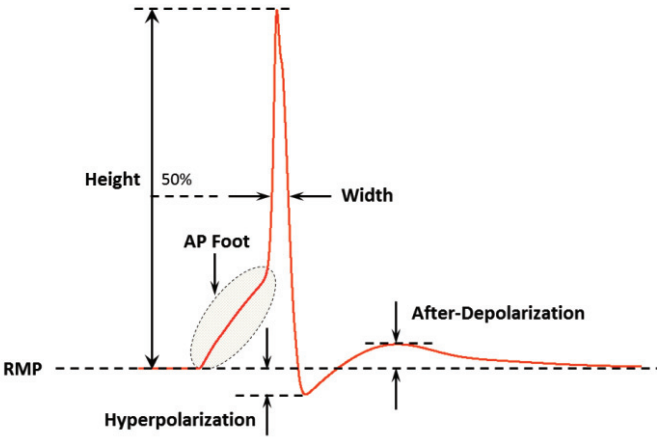

Figure 2: Parameters employed for quantifying action potential shape

(i) *Height*: Depolarization (in mV) from the resting membrane potential (RMP) to the peak of the spike

(ii) *Width*: Time (in ms) between the crossing of 50% height during the rising and falling phase of the spike

(iii) *Convexity*: Gives a measure of the convexity of the foot of the AP; the foot being defined as the phase of the AP from the initiation of depolarization (start point) to some point below the threshold (end point). This was quantified as the area between the AP curve and the straight line between the above two points, as shown in fig.4.

(iv) *Hyperpolarization*: Difference (in mV) between the RMP and the most hyperpolarized value of V_m following the peak of the AP

(v) *After-Depolarization*: Difference (in mV) between the most depolarized value of V_m, following the above point of hyperpolarization, and the RMP

The above parameters, convexity aside, are self-evident in their definitions. For measuring the convexity, we took into consideration other approaches as well. One of the conventional alternatives was to evaluate the curvature along the AP curve using the following equation:

$$Curvature = \frac{1}{Radius} = \left| \frac{y''}{\left(1 + y'^2\right)^{3/2}} \right| \qquad \text{(Eq. 4)}$$

where $y'$and y'' are the first and second derivatives of the AP, respectively. This translates points of maximum local convexity and concavity to local minima and maxima, respectively. It assigns maximum convexity to regions having maximum negative curvature, which do not suit the requirements of our study. For example, in certain scenarios, though the signal may exhibit high curvature, it lasts for a short duration and, more importantly, does not contribute in raising V_m towards threshold. Fig. 3(a) illustrates this, where it has been verified that the AP occurrence is independent of the synaptic activity causing the depolarization with high curvature in the AP foot. Also there are instances where the maximum convexity is identified at more depolarized values beyond our region of interest, as in fig. 3(b), and thus not characterizing the foot of the AP. As the signals vary in their shapes, variable number of convexities and concavities arise even when restricting our search between the start and the peak of the AP. Another approach to quantify convexity by evaluating the inflection point, also failed under similar circumstances owing to variable number of curvature changes. This prevents the application of a universal method as varying shapes require to be treated differently.

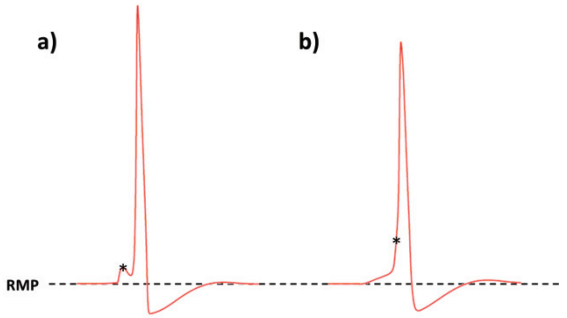

Figure 3: Issues with curvature as a measure of convexity. * indicates the location of maximum curvature.

In view of the above considerations, a novel approach of quantifying the foot convexity was developed taking into account a larger spread of V_m values. This involved evaluating the area between a pre-defined line and the AP foot as shown in Fig. 4. In determining the area, it is necessary to ensure that equal time frames of data are considered for each signal, to avoid errors due to differing rates of depolarization; some signals rise fast whereas others follow a much slower time course. We fixed the end-point first, selected as the average of peak concavity points determined using eq. 4 (observed before AP peak) from the entire set of APs. The maximum width between this point and the point of

initial crossing of 0.1 mV depolarization, calculated amongst all the signals, was set as the frame width. For each signal, the region of interest now extended for one frame width preceding the end-point, and the area evaluated between the AP curve and the straight line connecting the above two points. Our approach ensures better quantification of the foot convexity by not being overly influenced by acute features.

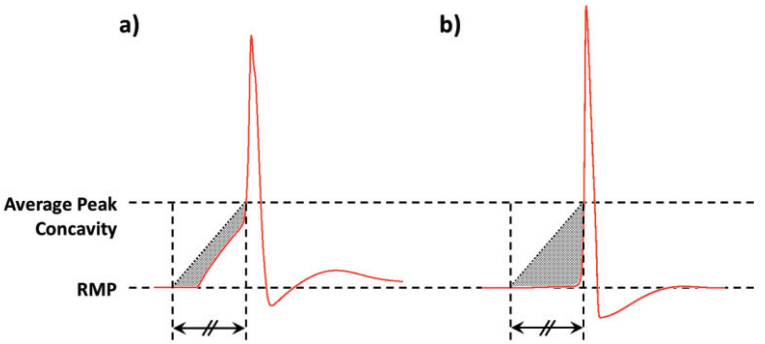

Figure 4: Method adopted to quantify convexity of AP foot. The shaded area indicates the area between the AP curve and the straight line joining the two defined points.

3 Results

3.1 Changes in Spike Shape with Propagation in a Syncytium

Notable differences can be observed in the shape of the individual spikes when stimulated, via synaptic stimulus, at the centroid cell of the syncytium. Three of these have been illustrated in fig. 5. All APs were analyzed for our parameters of interest and this has been summarized in table 1. AP height was found to vary by over 35 mV between APs recorded at various locations, along with significant differences in their widths. The largest heights were found to occur at the vertices followed by the surface cells while the cell initiating the AP produced the smallest heights. APs at the site of initiation always had the largest widths. Convexity in the foot of the AP was observed mainly at the site of initiation, and to an extent at the immediately neighboring cells. Consequently, majority of the cells tended to have a more concave rise to the AP peak. Cells close to the site of AP initiation were found to exhibit a lower level of hyperpolarization and a higher after-depolarization.

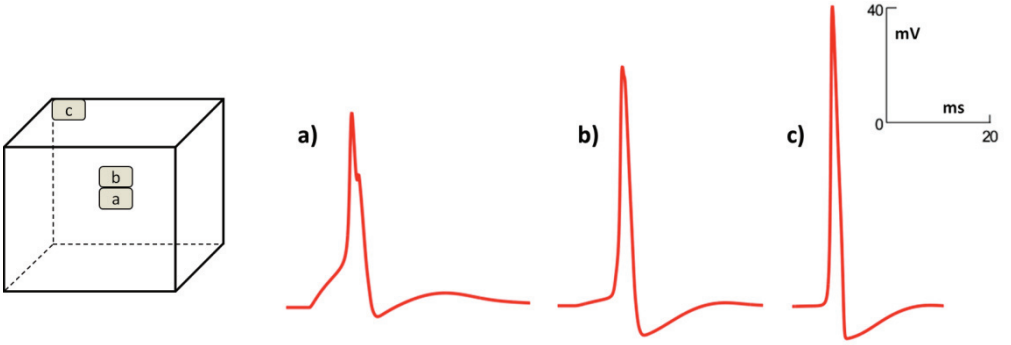

Figure 5: Examples of variety in AP shapes observed in a 5-cube syncytium when stimulated at the centroid. Cube on the left illustrates the location from where each recording was obtained.

From above it can be gauged that most of the AP features share strong correlations. We evaluated the correlation coefficients between all pairs of features. AP height was found to have strong negative correlations (–0.9) to width and convexity. A strong negative correlation (–1.0) also exists between the extent of hyperpolarization and after-depolarization. Strong correlations (0.9) are present between the AP width and the level of after-depolarization, and a negative correlation (−0.9) with the extent of hyperpolarization.

Parameter	Min	Max
Height (mV)	68.23	105.37
Width (ms)	1.53	2.58
Convexity	–46.98	–16.96
Hyperpolarization (mV)	3.15	11.17
After-Depolarization (mV)	0.51	5.10

Table 1: Range of AP parameters

3.2 Differences in Propagation Velocity

The syncytial nature also holds influence over other emergent properties such as the propagation velocity of APs. To investigate the syncytial effect on propagation it was deemed appropriate to focus on syncytia of larger sizes so as to observe a wider spatial profile, and thus syncytia of sizes 15- and 25- cube were considered.

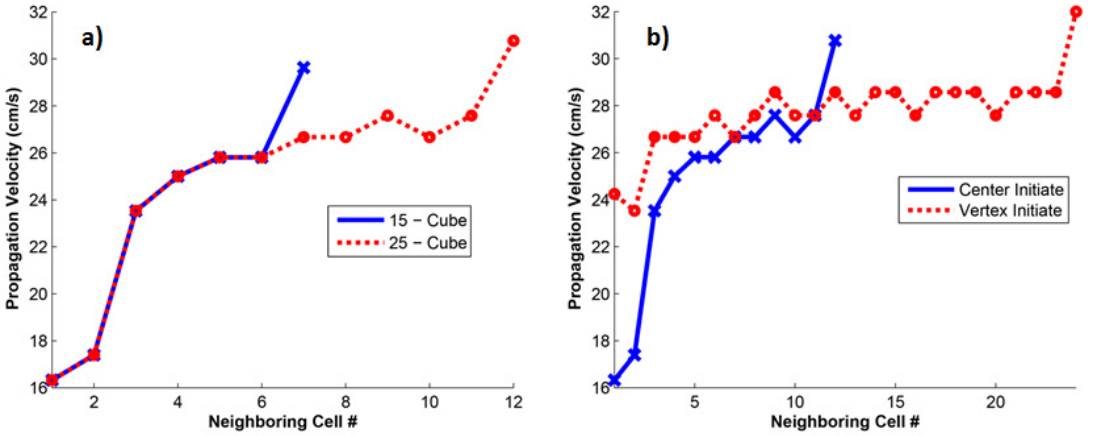

Figure 6: (a) Variation of propagation velocity of AP, initiated at the centroid cell in a syncytium of size 15-cube (solid blue) and 25-cube (dashed red). (b) Variation of propagation velocity in a syncytium of size 25-cube when initiated at the centroid cell (solid blue) and at the vertex cell (dashed red)

It was found that for APs originating at the centroid cell, the propagation velocity along the longitudinal axis is initially low (16.3 cm/s), then rises rapidly to plateau out (at around 26 cm/s) over most of the interior cells, before attaining a higher velocity (30.7 cm/s) close to the syncytial boundary (fig. 6a). Thus, propagation velocity is found to vary by as much as 90% over the syncytium. In contrast, for APs initiated at the vertex cell of the syncytium, the propagation velocity starts off at a relatively higher value before following the same trend (fig. 6b). Here, the overall variation is found to be only 32%, with the plateau at a slightly higher velocity of 28 cm/s. The conduction velocities across the transverse axes are comparatively much lower (plateau of 0.9 cm/s as compared to 26 cm/s) owing

to the smaller intracellular distances (cell diameter << cell length), but a similar trend in the variation of the conduction velocity is observed.

3.3 Spike Propagation in a Syncytium

Above we restricted our focus to the classical Hodgkin-Huxley action potentials. As syncytial tissues express action potentials of a wide variety, it would be relevant to explore variations in spike shapes with regards to their capacity to propagate in a syncytium. We explored ModelDB (Hines, Morse, Migliore, Carnevale, & Shepherd, 2004), a repository for computational models, for published models of action potentials that showed good contrast to the HH type, and selected an atrial cell model (accession number: 3800) (Courtemanche, Ramirez, & Nattel, 1998).

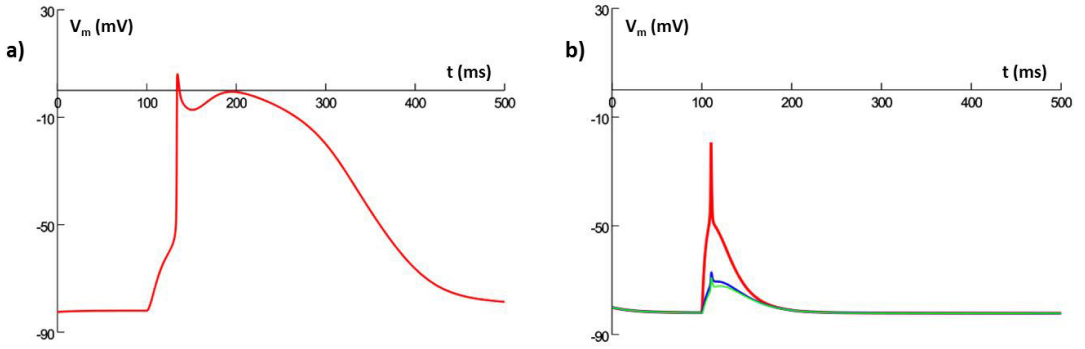

Figure 7: Action potential produced using spike mechanism from atrial cell model in (a) a single isolated cell, (b) a syncytium

As seen in fig. 7a, it had a huge time course (+300 ms) and a biphasic shape – a sharp rise followed by a notch and then a subsequent depolarization, before re-polarizing towards RMP. The RMP itself was more negative than for HH (–82 mV vs –65 mV). This spike mechanism was incorporated into each cell in our syncytium, and a synaptic stimulus was applied to the centroid cell. The response of the centroid cell (in red) and two of its immediate neighboring cells is shown in fig. 7b. It is evident that the spike failed to propagate and its shape in the centroid cell itself was markedly different from that seen in the single isolated cell model. The spike now displayed only a monophasic rise, with a reduced peak, and a much shorter time course (< 100 ms).

4 Discussion

Action potentials are generally referred to as all-or-none signals that propagate without change in amplitude or shape. Though this holds true when APs are compared against graded potentials, it fails under certain conditions. Even in long and continuous axons or muscle fibers, APs do exhibit differences in their shape while propagating away from the point of initiation – the most notable change lying in the foot of the AP, the rise to threshold, as illustrated in Fig. 8. It has been experimentally demonstrated that with increasing distance from the end-plate, the AP height increases and foot gradually turns from convex-upwards to concave-upwards (Fatt & Katz, 1951).

The results presented here provide ample evidence of the syncytial influence in determining the observed spike shape. We were able to demonstrate the origin of diverse spike shapes from a single basic underlying mechanism. This provides strength to the argument that, in the detrusor, only a few distinct spiking mechanisms may exist and their syncytial modulation is responsible for the wide variety in observed AP shapes. As action potentials are the precursors to muscle contraction, variations in their propagation velocity can have serious implications for producing coordinated

bladder contractions. We have seen here how the propagation velocity can also be dependent upon the site of AP initiation as well the location of the recording cell. Also, it was found that the shape of the AP may determine its ability to propagate through a syncytium, thereby differentiating between localized and coordinated contractions.

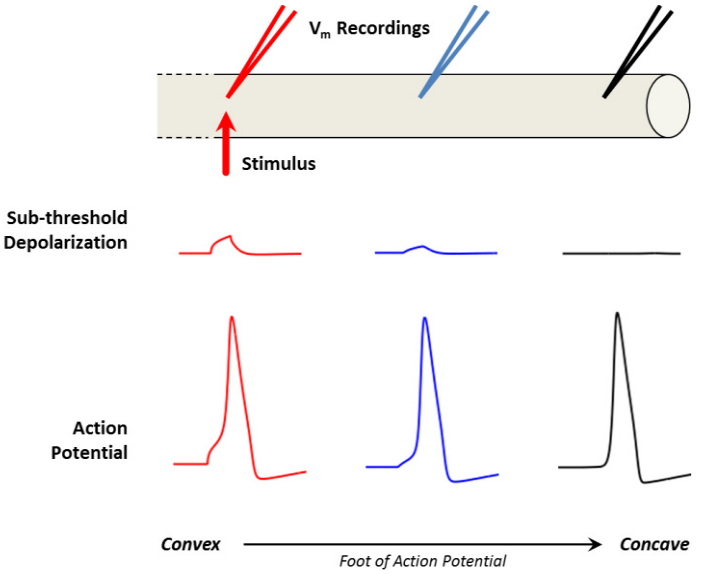

Figure 8: Change in the action potential foot while propagating along a long thin uniform cable

It should be kept in mind that the HH formalism, employed here, essentially consists of just two different ions with a single type of voltage-gated channel for each. In the case of the detrusor smooth muscle, the system deals with a large ensemble of ion channels, with multiple channel types for most ions. Some of these are voltage-gated (e.g. L-type Ca^{2+}, T-type Ca^{2+}) whereas others additionally also being ligand-activated (e.g. Ca^{2+} activated BK, IK, SK). Furthermore, intracellular calcium dynamics exerts a significant influence over the behavior of these channels. Thus, there is there even greater scope for variations in the observed spike shape.

In experimental studies, generally, data obtained from all intercellular recordings in a tissue are clubbed together and statistically analyzed. In view of the results presented here, it would be wiser to classify the cells into groups based on similarities in their electrical activity, which might correspond to likeness in the cellular environments, and subsequent analysis of these cell groups. By analyzing the electrophysiological recordings observed in health and pathology, we can characterize the spike shapes and their occurrence. For instance, in pathology leading to better intercellular coupling, there is likely to be a larger proportion of spikes with lower AP foot convexity, corresponding to propagated spikes. Studies on the origin of different spike shapes, and their variations in health and disease, may potentially offer significant insight into changes that take place at the cellular level under pathology and thus direct approaches to their treatment.

Acknowledgement

The work was supported by grants from the Department of Biotechnology (DBT), India (BT/PR14326/Med/30/483/2010) and the UKIERI (UKUTP20110055). The authors would like to thank Michael Hines and Ted Carnevale (Yale University) for their expert support with NEURON.

Conflict of Interest

The authors declare that they have no conflict of interest.

References

Andersson, K.-E. (2011). Antimuscarinic mechanisms and the overactive detrusor: an update. *European urology, 59*(3), 377-386.

Appukuttan, S., Brain, K. L., & Manchanda, R. (2014). A computational model of urinary bladder smooth muscle syncytium. *Journal of computational neuroscience*, 1-21.

Bennett, M., Gibson, W., & Poznanski, R. (1993). Extracellular current flow and potential during quantal transmission from varicosities in a smooth muscle syncytium. *Philosophical Transactions of the Royal Society of London. Series B: Biological Sciences, 342*(1300), 89-99.

Brading, A., & Brain, K. (2011). Ion channel modulators and urinary tract function. In *Urinary Tract* (pp. 375-393). Springer.

Carnevale, N. T., & Hines, M. L. (2006). *The NEURON book.* Cambridge University Press.

Courtemanche, M., Ramirez, R. J., & Nattel, S. (1998). Ionic mechanisms underlying human atrial action potential properties: insights from a mathematical model. *American Journal of Physiology-Heart and Circulatory Physiology, 275*(1), H301--H321.

Fatt, P., & Katz, B. (1951). An analysis of the end-plate potential recorded with an intra-cellular electrode. *The Journal of physiology, 115*(3), 320-370.

Fry, C. H., Skennerton, D., Wood, D., & Wu, C. (2002). The cellular basis of contraction in human detrusor smooth muscle from patients with stable and unstable bladders. *Urology, 59*(5), 3-12.

Fry, C., Cooklin, M., Birns, J., & Mundy, A. (1999). Measurement of intercellular electrical coupling in guinea-pig detrusor smooth muscle. *The Journal of Urology, 161*(2), 660-664.

Hayase, M., Hashitani, H., Kohri, K., & Suzuki, H. (2009). Role of {K}+ Channels in Regulating Spontaneous Activity in Detrusor Smooth Muscle In Situ in the Mouse Bladder. *The Journal of Urology, 181*(5), 2355-2365.

Hines, M. L., Morse, T., Migliore, M., Carnevale, N. T., & Shepherd, G. M. (2004). ModelDB: a database to support computational neuroscience. *Journal of computational neuroscience, 17*(1), 7-11.

Jack, J. J., Noble, D., & Tsien, R. W. (1975). *Electric current flow in excitable cells.* Clarendon Press (Oxford).

Manchanda, R. (1995). Membrane Current and Potential Change During Neurotransmission in Smooth Muscle. *Current Science, 69*(2), 140-150.

Neuhaus, J., Wolburg, H., Hermsdorf, T., Stolzenburg, J.-U., & Dorschner, W. (2002). Detrusor smooth muscle cells of the guinea-pig are functionally coupled via gap junctions in situ and in cell culture. *Cell and Tissue Research, 309*(2), 301-311.

Purves, R. (1976). Current flow and potential in a three-dimensional syncytium. *Journal of Theoretical Biology, 60*(1), 147-162.

Rall, W. (1964). Theoretical significance of dendritic trees for neuronal input-output relations. *Neural Theory and Modeling*, 73-97.

Sourav, S., & Manchanda, R. (2000). Influence of the size of syncytial units on synaptic potentials in smooth muscle. *Medical and Biological Engineering and Computing, 38*(3), 356-359.